DOI: 10.61782/fa.2025.0541

FORUM ACUSTICUM
EURONOISE 2025

MACHINE LEARNING-BASED MODELLING OF UAV NOISE METRICS IN REAL CONDITIONS

Camilo I. Andino Cappagli[1*] **Alireza Amiri-Simkooei**[1] **Salil Luesutthiviboon**[1]
Tomáš Meiser[2] **Amy Morin**[1] **Michal Zajačík**[2]
Milan Rollo[2] **Mirjam Snellen**[1]
[1] Operations and Environment section, Faculty of Aerospace Engineering,
Delft University of Technology, Netherlands
[2] AgentFly Technologies, Prague, Czechia

ABSTRACT

Over the last decade, there has been a marked increase in the use of drones for various applications including emergency and natural disaster response, payload delivery, aerial imaging and surveillance. There are currently many private and public initiatives that aim to further increase the number of drones and diversify their tasks, offering many associated benefits such as reduction in emissions by replacing traditional and more polluting options with electric unmanned aerial vehicles (UAVs). However, several challenges have to be addressed before a broader implementation is accomplished. One of such challenges is the reported noise annoyance produced by UAVs. This study focuses on the development of data-driven models to predict the dynamics of noise metrics during real UAV operations. Extensive outdoor experimental campaigns were conducted, where array-based measurements were recorded during several manoeuvres performed by different types of drones. Beamforming techniques were applied to improve data quality and signal-to-noise ratio (SNR), and to synchronize telemetry and acoustics data streams. Using the improved experimental data, an initial machine learning model was developed to predict the back-propagated $OSPL$ as function of telemetry-derived operational parameters for ascent, hover, and descent. The model managed to accurately predict the experimental data, and it was found that the elevation angle was the most important predictor of $OSPL$ for the considered manoeuvres.

Keywords: Drones, noise metrics, noise prediction, machine learning models

*__Corresponding author__: c.i.andinocappagli@tudelft.nl.
__Copyright__: ©2025 Camilo I. Andino Cappagli et al. This is an open-access article distributed under the terms of the Creative Commons Attribution 3.0 Unported License, which permits unrestricted use, distribution, and reproduction in any medium, provided the original author and source are credited.

1. INTRODUCTION

Several factors have led to a sharp increase in the number of drones and tasks, some of which are due to the reduction of production costs, the development of more efficient and smaller technologies, critical for the manufacturing and control of these systems, and their versatility performing a large variety of tasks. Among these, photography and video recording capabilities have enabled drones to support, for example, infrastructure development and surveillance and security. Drones have also been employed to provide assistance in emergencies and natural disasters, in agricultural applications, and goods transportation [1]. Generally, they are considered to have great potential to serve as greener and more sustainable options to replace traditional, more contaminating methods. The number of tasks that UAVs can perform exceeds this list, but the critical natures of certain applications signify their importance.

However, one of the main barriers to the broader adoption and applications of UAVs is the reported acoustic annoyance caused by their operation [2–4]. To allow for the sector to sustainably grow, it is essential to address such reported acoustic annoyance. A predictive tool is needed to estimate representative psychacoustic metrics. Given the wide range in drone types and operational conditions, outdoor drone noise measurements are considered an important element in the efforts of working towards such a tool. These need to be developed based on studies of typical real UAV operations to understand the connections between operational parameters and the acoustics, as well as the influence of environmental factors.

The resulting tools will allow for adequate mission planning, manoeuvre optimization, and design improvements to mitigate acoustic annoyance. As the acoustics vary for different drone types and manoeuvres, these differences must be taken into account as well. At the same time, these tools need to remain computationally inexpensive for fast calculations and seamless

integration into optimization frameworks. Studying drone noise with the drone operating under realistic conditions is essential to ensure a realistic overview of the expected noise. Recent studies have explored UAV noise in such realistic and uncontrolled environments [5–7]. These works focused on measuring and characterising noise from specific drones under realistic conditions. In this study, we describe the development and initial results of a data-driven model that managed to predict experimentally measured acoustic features using telemetry-based variables, and identified important operational parameters as main predictors.

2. METHODS

2.1 Experimental campaigns

An experimental campaign was conducted in April 2024 at an airfield on the outskirts of Prague, Czechia. The site was chosen for its isolation from populations centers, and it was only close to a seldom-used road. Additionally, the airspace in the area was not crowded by air traffic, with only a few aircraft flying overhead throughout the campaign. These occurrences were noted in the experimental logs to account for their contributions, or remeasure if necessary. Taken all together, these conditions met the site goal which was to constitute a highly isolated environment in terms of additional noise sources, while still being an outdoor environment with its inherent variability, including occasional wind currents and gusts. The tested flight plan consisted of a series of manoeuvres including ascent, hover, descent, horizontal flights, and sudden changes in direction. All manoeuvres were performed by three different multirotor UAVs.

To start the model development, operations involving ascent, hover, and descent were analysed. Each operation was performed as follows: The drone took off and ascended vertically to 10 m above ground level (AGL), where it hovered for 15 seconds. It then ascended to 30 m where it hovered again for the same duration, and repeated the process at 50 m and 70 m. Once the hover at the last altitude was completed, the drone descended continuously until landing. The altitude profile, as a function of time, for this operation is shown in figure 1.

This operation was repeated for five different take off positions, where the ascent position, relative to the microphone array, was changed. The take off positions were located north, south, west, and east of the microphone array, at approximately 25 m distance, and an additional site at 50 m east of the array, resulting in five total take off positions. The combined altitude profile of these operations can be observed in figure 2. Differences in altitudes corresponding to different operations occurred due to pilot operations. The selected drone was a co-rotational (X8) quadcopter Gorgon, built, developed, and piloted by AgentFly Technologies, which can be observed in figure 3.

To measure the acoustic signal while the manoeuvre was performed, an array of 4 m of aperture, consisting of 64 microphones, with a sampling frequency of 62500 Hz was used. To attenuate ground reflections, a foam was placed under the entire array, and a secondary foam was placed in the central part of the array between the microphones and the array structure to avoid these reflections, had they appeared.

To record the operational parameters of the drone, the autopilot telemetry and ESCs were used. Among several others, these included the GPS-based information, position, velocity, and acceleration, the RPMs of individual rotors, and thrust, all recorded as a function of time.

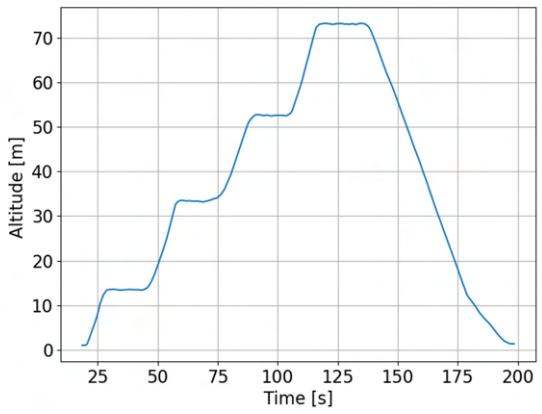

Figure 1. Altitude profile for a single ascent-hover-descent operation performed by the Gorgon X8.

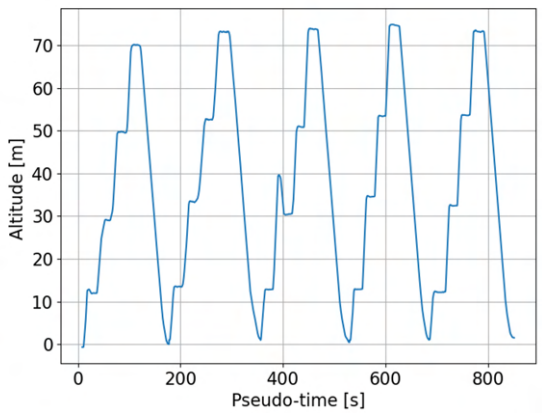

Figure 2. Altitude profile for five ascent-hover-descent operations performed by the Gorgon X8. The horizontal axis represents a sequential arrangement of time-series data rather than the actual time. Variability among signals is evident due to the manual piloting of these operations.

Figure 3. Photo of the selected drone, Gorgon X8, developed and operated by AgentFly Technologies. Credits: Dr. Milan Rollo, AgentFly Technologies.

2.2 Beamforming techniques

Given the goal of developing a data-driven model to describe the time dynamics of different acoustic metrics, it is necessary to first address two points. i) As explained in the previous section, different measures were taken to reduce the effect of ground reflections. However, it was impossible to eliminate them entirely during the data acquisition. ii) It is important to accurately synchronize all telemetry variables and acoustic data to increase the model validity. This involves both properly synchronizing the data and correcting the GPS readouts due to their uncertainties. To address the above issues, beamforming was used.

To do this, a beamformer for a fixed source position ξ_j is defined based on the following functional structure [8]:

$$B(r,\theta,\phi) = \frac{\mathbf{g}_j^* \langle \mathbf{p}\mathbf{p}^* \rangle \mathbf{g}_j}{|| \mathbf{g}_j ||^4} \tag{1}$$

where $\langle \mathbf{p}\mathbf{p}^* \rangle$ is the Cross-Spectral Matrix (CSM) of the measured pressures, which is generated by averaging the Fourier transforms of sample blocks of 0.1 s in our case, with no overlap considered, and $\mathbf{g}_j^*$ is the steering vector

$$g_{j,n} = \frac{\exp\left(-2\pi i f \Delta t_{j,n}\right)}{4\pi \, || \, \mathbf{x}_n - \xi_j \, ||} \tag{2}$$

with $\Delta t_{j,n}$ the delay between the emission at the position ξ_j and the receiver position $\mathbf{x}_n$. The beamformer (1) establishes a correlation between the actual location information of the source, contained within the CSM, and the source position considered, represented by the steering vector in Equation 2. By considering many potential source locations ξ_j, the location corresponding to the maximum of Equation 1 is used as the estimate of the source position from the array measurements.

This methodology was used to reconstruct the UAV trajectory, independent from the GPS information. Then, the acoustic localization-based and GPS-based trajectories were compared to estimate the corrections needed in the GPS telemetry data.

Once the corrections were implemented, the steering vector was no longer defined based on the estimated position, but rather in terms of the GPS-corrected trajectory. As the beamforming considers all microphones, while compensating for delays to effectively focus on the source, it generates a much cleaner spectrogram with improved SNR compared to single microphone measurements. Once the beamformed spectrogram was obtained, the signals were back-propagated for each beamformed frequency band according to:

$$SPL_{source}(f,t) = SPL_{ground}(f, t + \frac{r(t)}{c}) \tag{3}$$

$$+20 \log \frac{r(t)}{r_0} + \alpha(f) r(t) \tag{4}$$

where r is the distance between the array and the drone, $r_0 = 1$ m, c the sound speed, and $\alpha(f)$ is the coefficient of atmospheric absorption, which depends on the frequency, and also on relative humidity and temperature, both of which were recorded during the measurement campaign.

This procedure generated a cleaner, back-propagated to the source spectrogram, where ground reflections are attenuated. The single microphone and beamformed spectrograms for a single operation can be observed in figure 4

3. RESULTS

3.1 Correlation study

From the telemetry data, different observables were computed as inputs for the data-driven models. These were:

- Azimuthal angle $\phi(t)$: The angular position between the microphone array and the drone measured on the horizontal plane (on the ground).
- Elevation angle $\theta(t)$: The polar angle between the microphone array and the drone, with $\theta = 0$ when the drone is on the ground, and $\theta = \frac{\pi}{2}$ if the drone is overhead.
- Velocity vector absolute value $|\bar{v}(t)|$
- Acceleration vector absolute value $|\bar{a}(t)|$
- Thrust percentage T
- Each of the eight rotors rpm $\{n_{p,i}(t)\}_{i=1\ldots8}$

As the acoustic metrics were back-propagated to the source hemisphere, the range between the array and drone and altitude were not considered.

Since ascent, hover, and descent were the initially tested maneuvers, it is expected that under isolated, ideal conditions, all rpms should have the same absolute value at corresponding times. In the cases of ascent and descent, the absolute rpm of all rotors should be identical at each moment, whereas for hover,

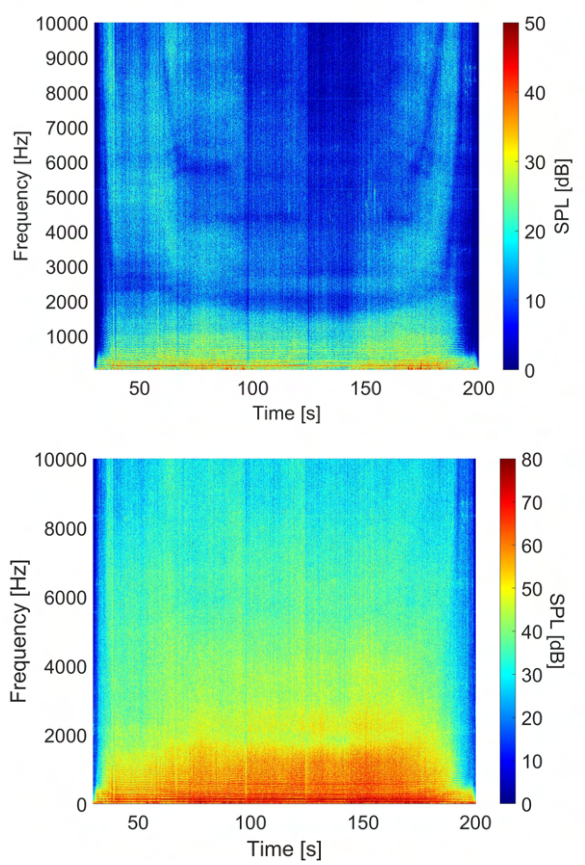

Figure 4. Top: Single microphone spectrogram from an ascent-hover-descent operation. Despite the measures taken during the experiments to attenuate reflections, some effects are still clear. These reflections however, do not appear to be due to ground effects but rather from the outermost parts of the array, which appear to act as spurious sources. Bottom: Beamformed spectrogram from a single ascent-hover-descent operation. Compared with the top, the reflections are greatly attenuated. The dB values increase as this spectrogram is back-propagated to the source. The tones are clearer than the top frame, and in particular, they are present up to 2 kHz. In this range, and for higher levels, the noise is dominated by its broadband component.

the rpm of all rotors would remain constant also during the duration of the manoeuvre. Therefore, the rpms time series were replaced, and the following observables were generated:

$$\langle n_p(t)\rangle = \frac{1}{N_r}\sum_{i=1}^{N_r} \mid n_p(t) \mid \tag{5}$$

$$\sigma_{n_p}(t) = \sqrt{\frac{1}{N_r}\sum_{i=1}^{N_r}(\mid n_p(t) \mid -\langle n_p(t)\rangle)^2} \tag{6}$$

where the average and standard deviations were calculated at equal times, thereby resulting in time series as well.

The $\langle n_p(t)\rangle$ measures the overall rpm, and $\sigma_{n_p}(t)$ is used to quantify how far from the ideal hover, ascent or descent the rpm activities are; a value of $\sigma_{n_p}(t_i) = 0$ indicates that at the time t_i, all the rotors had the same rpm. In other words, variations given by factors such as wind gusts and pilot-induced perturbations will cause this observable to vary from zero. The time over which each effect takes place depends on factors such as pilot reaction time, and wind gust intensity and duration.

The first step towards studying relations between both sets of variables (acoustic metrics and telemetry data) was to compute pair-wise correlations between each of the inputs and $OSPL$, considering a single ascent-hover-descent operation. The Spearman correlation was used as it can test for the existence of general monotonic correlations. The results are shown in figure 5.

As it can be observed from the correlation coefficients, the correlation between the $OSPL$ and the elevation angle θ is significantly increased. To validate the results, Pearson correlation was also used and displayed approximately the same coefficient between both of these variables (data not shown).

This study is a sufficient condition to establish that the elevation angle is a variable of importance to predict the $OSPL$, but it does not necessarily mean that the other variables are not relevant, as this is a pair-wise study and does not capture any coupling between input variables. Additionally, both metrics have limitations, with Spearman correlation allowing for non-linear but monotonic relations, and Pearson looking exclusively to linear relations; both could be excluding the discovery of more complex relations.

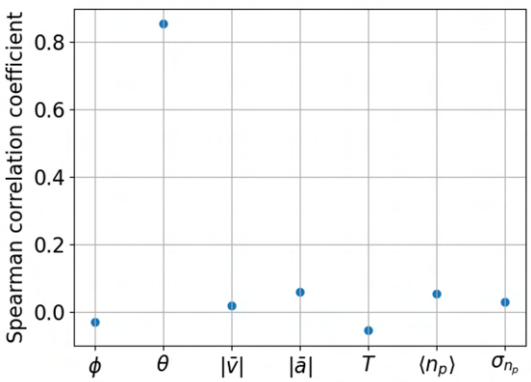

Figure 5. Spearman correlation of the $OSPL$ with each of the tested input parameters. A considerable increase is observed for the elevation angle. This implies the existence of a monotonic relation between both signals.

3.2 Model results

Because drone operations in uncontrolled environments tend to show a higher variability in terms of the drone flight dynamics and therefore in the generated acoustic signals, it is important to understand the model performance in representing this variability. To this end, all five ascent-hover-descent operations were integrated together into the dataset for the model. The altitude profile corresponds in this case with the one observed in figure 2 in the section 2.1.

As the correlation analysis showed that relations exist between at least one of the telemetry variables considered and the measured $OSPL$, the main goal was to find such relations and use them to predict this acoustic metric. To create a model capable of capturing complex relations between the operational parameters and the acoustic metrics, machine learning techniques were employed. In this work, we report the model results for the case of random forest regression (RFR). This method was chosen after comparing the prediction accuracy of different ML regression models, from which RFR proved to be the most accurate while remaining relatively simple. Additionally, Random Forest has also been used in other works related to assesment and prediction of aviation noise [9].

Initially, a series of studies were performed to optimize the number of decision trees. The optimization consisted of generating training, validation, and quality assessment of prediction procedures for each number of decision trees. Randomization and splitting were done before the optimization starts; dividing the randomized data into 80% training and 20% for validation. After the model for each number of trees is trained on the training set, the prediction is computed by applying it to the validation data and generating the model estimation. R^2, $RMSE$, and MAE were calculated based on the prediction and stored for each decision trees number. The optimal number of decision trees was set based on the highest value of R^2. It was also checked that the values of $RMSE$ and MAE have a local minimum at the chosen value. These results can be observed in the figures 6, 7, 8.

The optimization resulted in an optimal number of trees, which was then used to produce the optimal model predictions, which can be observed in figures 9 and 10, and the accuracy in figure 11. From figure 10, the dynamics of the $OSPL$ is accurately recovered by the model. There are sources of deviations arising from extreme values and stochastic experimental noise.

To assess the robustness of the model results, the optimization was repeated for different randomization of the dataset and the R^2, $RMSE$, and MAE were extracted again. No significant difference was observed for the optimized model, presenting similar values up to the 3 decimal place of R^2. The results obtained from the initial optimization are then robust relative to changes in the data randomization. Therefore, the model managed to generate accurately predictions of the experimentally obtained $OSPL$ when all operations are considered together.

To assess the relevance of each of the input variables to predict the $OSPL$, the feature importance of the model was studied, analyzing the mean decrease impurity (MDI). This metric measures how much each input variable reduces the variance of the target values after it is used to split the data. The results from

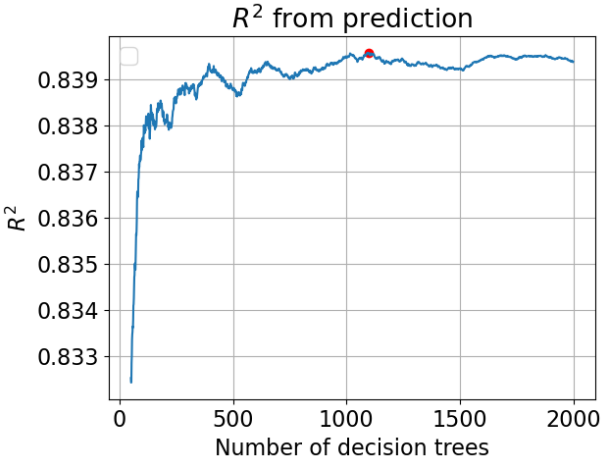

Figure 6. Optimization of the number of decision trees based on the highest R^2. In red, this maximum is shown. It can be observed that the variations on the R^2 are small, as it only changes a maximum of 0.007.

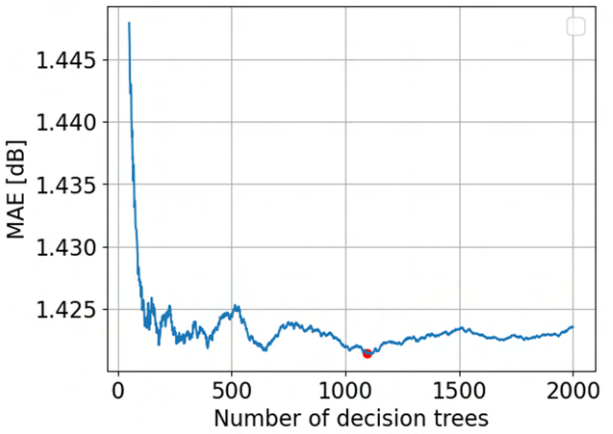

Figure 7. Values of the MAE calculated on the model prediction from each optimization run based on the highest R^2. In red, the number of decision trees for which the highest R^2 is obtained is displayed. It was observed that it corresponded to a local minima of the function. The variation on the MAE is small, with a maximum of 0.025 dB.

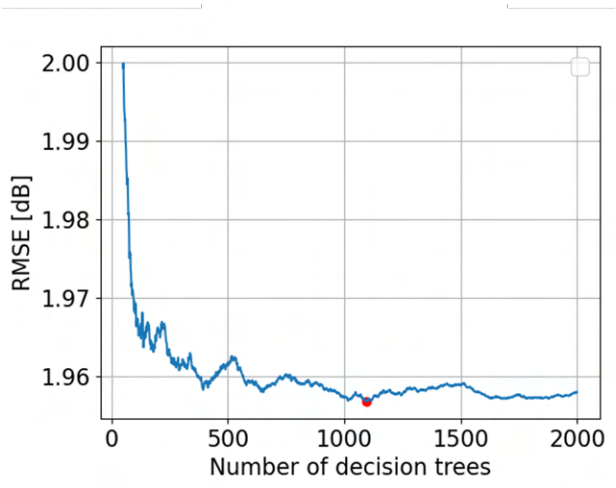

Figure 8. $RMSE$ of the prediction from each optimization run based on the highest R^2. In red, the number of decision trees for which the highest R^2 is obtained is displayed. The variation on the $RMSE$ is small, with a maximum of 0.05 dB across all tree values.

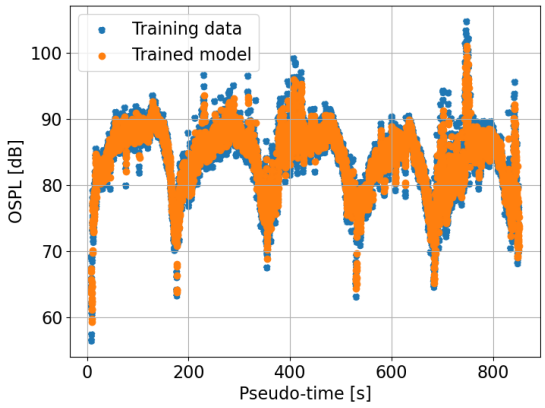

Figure 9. Trained RFR of the $OSPL$ data using the optimal number of decision trees.

this analysis can be observed in figure 12

As the MDI results show, the elevation angle results in the most important predictor of the $OSPL$, which implies that the information of both the $OSPL$ dynamics and intensity can be greatly explained by the elevation angle. Since all acoustic data was back-propagated to the 1 m hemisphere, the elevation angle is the angle between the horizontal plane of the drone and the field point.

This result implies that the $OSPL$ hemisphere behaviour

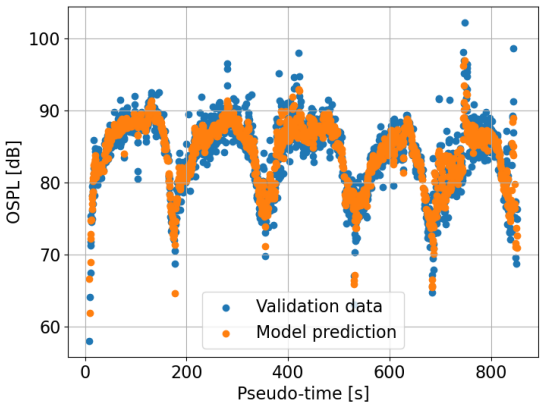

Figure 10. RFR prediction of the $OSPL$ using the optimal number of decision trees.

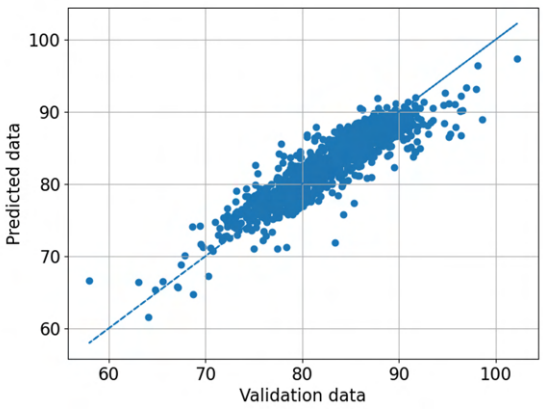

Figure 11. RFR prediction of the OSPL plotted as function of the validation data, for the case where all the operations were used. The model manage to capture most of the behaviour of the $OSPL$, with $R^2 = 0.84$

takes over other sound generating mechanisms when assessing predictor importance during realistic environmental conditions. The observed behaviour of the model in terms of R^2, deviation relative to the validation data, and feature importance, indicate that the prediction is accurate and robust to the high variability allowed. Furthermore, the ascent-hover-descent manoeuvres were performed manually, which adds a level of variability that is not usually present in systematic drone operations. Because of this, the model could show more accurate results when the automatic pilot commands the drone.

To visually verify the behaviour of the elevation angle, it

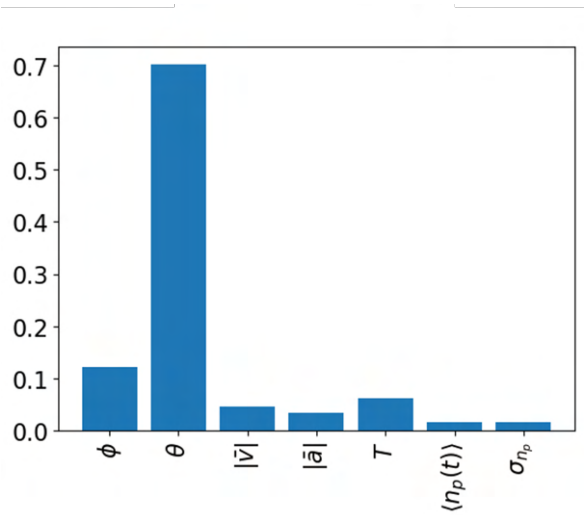

Figure 12. RFR parameter importance. The elevation angle scores the maximum MDI.

can be observed $OSPL$ for all the operations can be observed in figure 13.

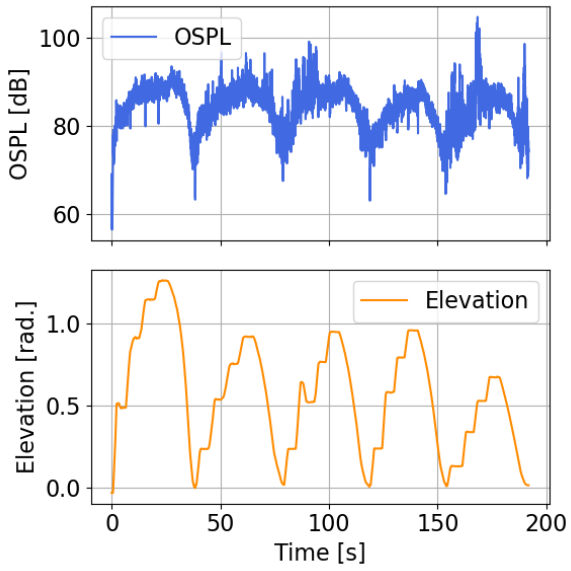

Figure 13. Comparison between the elevation angle (θ) and the $OSPL$ of all the ascent-hover-descent operations.

It is observed that the $OSPL$ increases as the elevation angle increases, which indicates that more frequency-integrated acoustic energy is measured when the field point is located closer to the bottom of the drone. As it can be observed in figure 13, this behaviour is not linear and the $OSPL$ increases more for smaller elevation angles, and it reaches an asymptotic behaviour for larger elevation angles.

4. CONCLUSIONS AND DISCUSSIONS

During the present work a machine learning model was developed and tested to predict the $OSPL$ caused by ascent, hover and descent operations of an X8 multirotor drone. The model managed to predict most of the variation observed in the acoustic metric calculated directly from experimental data, taken in realistic outdoor operational conditions. The elevation angle was found to be the most important predictor of the $OSPL$ in the tested manoeuvres, which indicates that the geometry of the hemisphere is more relevant than the other telemetry-based variables.

Consequently, the model is able to represent an effective geometry of the radiation lobe of the drone's $OSPL$. In particular, based on the observed non-linear behaviour, where the $OSPL$ increases more for smaller angles, and much less for larger angles, the model could indicate a sinusoidal/shifted-cosine dependency on the angle, which points at a dipolar behaviour of the sound propagation. This effect will be validated and further studied for other acoustic metrics in the future, as well as for the other manoeuvres and drones recorded during the experimental campaign.

This paper presents a method to generate predictions of total $OSPL$ prior to operations, involving ascent, hover, and descent. As these are critical manoeuvres for real UAV operations, they are highly relevant for assessing the impact of these operations on human populations nearby. During ascent and hover in real conditions, the drone has to accelerate or maintain an altitude, while adapting the rotors activities to compensate for any wind distortions, which in turn generate a fast variation of the acoustic dynamics. This first model managed to represent most of these variations based on telemetry-based features, accomplishing a good degree of accuracy and robustness, when analyzing all operations together.

Since the input features are directly derived from telemetry data, the model shows the potential to be also used as a way of interrogating the importance of physical drivers and guide the development of physics-based theories that can study from first principles, the dominant sound generating mechanisms in realistic, uncontrolled, conditions.

In a broader aspect, these results represent a first step into the development of a predictive tool to quantify the acoustic impact of drone operations. During the measurements campaign explained in section 2.1, several horizontal flight and changes in directions were measured, which are being used to extend the model to these different manoeuvres, hence more comprehensively studying a full flight envelope. To study how general the

predictors are, other multirotor systems that were used in the measurements campaign will be analysed.

Based on the measured manoeuvres, a series of uncertainty quantification studies are being developed with two objectives. Firstly, to quantify the accuracy of the model as well as its uncertainty for the different studied manoeuvres. Secondly, to study the role of wind gusts in the acoustic metrics and to quantify the effect on the model predictions.

5. ACKNOWLEDGMENTS

The authors are grateful to the EC for supporting the present work, performed within the REFMAP project, funded by the European Union's Horizon Europe research and innovation programme under grant agreement no. 101096698 (REFMAP). This publication solely reflects the authors' view and neither the European Union, nor the funding Agency can be held responsible for the information it contains.

6. REFERENCES

[1] C. Wankmüller, M. Kunovjanek, and S. J. Mayrgündter, "Drones in emergency response – evidence from cross-border, multi-disciplinary usability tests," *International Journal of Disaster Risk Reduction*, vol. 65, no. 102567, 2021.

[2] H. Eißfeldt and V. Vogelpohl, "Drone acceptance and noise concerns — some findings," in *20th International Symp. on Aviation Psychology*, (Dayton, Ohio, USA.), pp. 199–204, 2019.

[3] McKinsey and Company, *Study on the societal acceptance of urban air mobility in Europe*. EASA, 2021.

[4] D. Bajde, N. Woermann, M. H. Bruun, R. Gahrn-Andersen, J. K. Sommer, M. Nøjgaard, S. H. Christensen, H. Kirschner, R. H. Skaarup Jensen, and J. H. Bucher, *Public reactions to drone use in residential and public areas*. University of Southern Denmark / Aalborg University, 2021.

[5] C. Ramos-Romero, N. Green, A. J. Torija, and C. Asensio, "On-field noise measurements and acoustic characterisation of multi-rotor small unmanned aerial systems," *Aerosp. Sci. Technol*, vol. 141, no. 108537, 2023.

[6] N. Konzel and E. Greenwood, "Ground-based acoustic measurements of small multirotor aircraft," in *Vertical Flight Society's 78th Annual Forum & Technology Display*, (Fort Worth, Texas, USA.), 2022.

[7] T. Zhou, H. Jiang, and B. Huang, "Quad-copter noise measurements under realistic flight conditions," *Aerosp. Sci. Technol*, vol. 124, no. 107542, 2022.

[8] R. Merino-Martinez, P. Sijtsma, M.Snellen, T. Ahlefeldt, J. Antoni, C. J. Bahr, D. Blacodon, D. Ernst, A. Finez, S. Funke, T. F. Geyer, S. Haxter, G. Herold, X. Huang, W. M. Humphreys, Q. Leclère, A. Malgoezar, U. Michel, T. Padois, A. Pereira, C. Picard, E. Sarradj, H. Siller, D. G. Simons1, and C. Spehr, "A review of acoustic imaging methods using phased microphone arrays," *CEAS Aeronautical Journal*, vol. 10, pp. 197–230, 2019.

[9] J. Meister, "Power setting estimation of departing civil jet aircraft based on machine learning," *Journal of Aircraft*, vol. 61, no. 4, 2024.